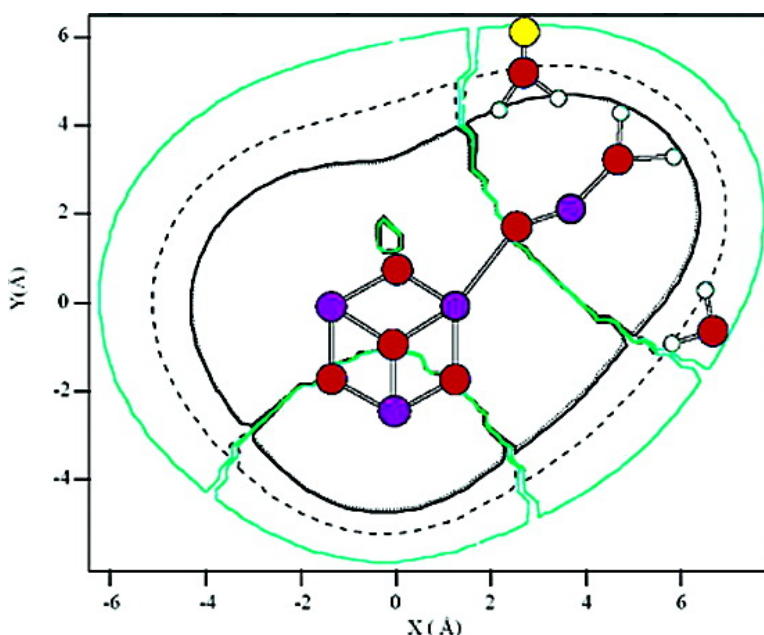


Investigation of the Calcium-Binding Site of the Oxygen Evolving Complex of Photosystem II Using Sr ESEEM Spectroscopy

Sun Hee Kim, Wolfgang Gregor, Jeffrey M. Peloquin, Marcin Brynda, and R. David Britt

J. Am. Chem. Soc., **2004**, 126 (23), 7228-7237 • DOI: 10.1021/ja030614e • Publication Date (Web): 22 May 2004

Downloaded from <http://pubs.acs.org> on March 31, 2009



More About This Article

Additional resources and features associated with this article are available within the HTML version:

- Supporting Information
- Links to the 2 articles that cite this article, as of the time of this article download
- Access to high resolution figures
- Links to articles and content related to this article
- Copyright permission to reproduce figures and/or text from this article

[View the Full Text HTML](#)



Investigation of the Calcium-Binding Site of the Oxygen Evolving Complex of Photosystem II Using ^{87}Sr ESEEM Spectroscopy

Sun Hee Kim, Wolfgang Gregor,[†] Jeffrey M. Peloquin,[‡] Marcin Brynda, and R. David Britt*

Contribution from the Department of Chemistry, University of California, Davis, California 95616

Received November 5, 2003; E-mail: rdbritt@ucdavis.edu

Abstract: The proximity of the calcium/strontium binding site of the oxygen evolving complex (OEC) of photosystem II (PSII) to the paramagnetic Mn cluster is explored with ^{87}Sr three-pulse electron spin-echo envelope modulation (ESEEM) spectroscopy. CW-EPR spectra of Sr^{2+} -substituted Ca^{2+} -depleted PSII membranes show the modified $g = 2$ multiline EPR signal as previously reported. We performed three-pulse ESEEM on this modified multiline signal of the Mn cluster using natural abundance Sr and ^{87}Sr , respectively. Three-pulse ESEEM of the natural abundance Sr sample exhibits no detectable modulation by the 7% abundance ^{87}Sr . On the other hand, that of the ^{87}Sr enriched (93%) sample clearly reveals modulation arising from the $I = 9/2$ ^{87}Sr nucleus weakly magnetically coupled to the Mn cluster. Using a simple point dipole approximation for the electron spin, analysis of the ^{87}Sr ESEEM modulation depth via an analytic expression suggests a Mn–Ca (Sr) distance of 4.5 Å. Simulation of three-pulse ESEEM with a numerical matrix diagonalization procedure gave good agreement with this analytical result. A more appropriate tetranuclear magnetic/structural model for the Mn cluster converts the 4.5 Å point dipole distance to a 3.8–5.0 Å range of distances. DFT calculations of ^{43}Ca and ^{87}Sr quadrupolar interactions on Ca (and Sr substituted) binding sites in various proteins suggest that the lack of the nuclear quadrupole induced splitting in the ESEEM spectrum of ^{87}Sr enriched PSII samples is related to a very high degree of symmetry of the ligands surrounding the Sr^{2+} ion in the substituted Ca site. Numerical simulations show that moderate ^{87}Sr quadrupolar couplings decrease the envelope modulation relative to the zero quadrupole case, and therefore we consider that the 3.8–5.0 Å range obtained without quadrupolar coupling included in the simulation represents an upper limit to the actual manganese–calcium distance. This ^{87}Sr pulsed EPR spectroscopy provides independent direct evidence that the calcium/strontium binding site is close to the Mn cluster in the OEC of PSII.

Introduction

Photosynthetic oxygen evolution results from a light-driven water oxidation process catalyzed by Photosystem II (PSII). The water oxidation chemistry occurs at the oxygen evolving complex (OEC), which consists of a tetranuclear Mn cluster and a redox active tyrosine, Y_Z (tyrosine 161 of the D1 protein).^{1–3} The oxygen evolution cycle involves five “S” states, S_0 – S_4 . Molecular oxygen is released following the formation of the final S_4 state as the OEC resets to the S_0 state.^{4,5} This water oxidation chemistry requires two ion cofactors, Ca^{2+} and Cl^- .⁶ However, the locations and the functional roles of these

ions still remain to be determined. Recently, progress has been made on obtaining crystal structures of PSII⁸ from *Thermosynechococcus elongatus* at 3.8 Å resolution^{8b} and from *Thermosynechococcus vulcanus* at 3.7 Å resolution.^{8c} Zouni et al.^{8b} provides assignments for the larger subunits and the locations and orientations of the cofactors. In particular, the partial resolution of the Mn cluster arises in the crystal structure. Zouni et al. positions three manganese ions at the corners of a triangle, with a fourth manganese ion placed near the center of the triangle, with interatomic distances about 3 Å. There are current Mn cluster models that fit within this general motif; for instance, our EPR/ENDOR based “Dangler” model predicts that the Mn cluster consists of a strongly antiferromagnetically coupled trinuclear core, with a fourth more weakly exchanged coupled manganese ion in close proximity.⁹

[†] Current address: Department of Basic Pharmacology, Veterinary University of Vienna, Wien, Austria.

[‡] Current address: Department of Chemistry, Boise State University, Boise, ID 83725-1520.

(1) Debus, R. J. *Biochim. Biophys. Acta* **1992**, *1102*, 269–352.

(2) Yocum, C. F. *Biochim. Biophys. Acta* **1991**, *1059*, 1–15.

(3) Britt, R. D. In *Oxygenic Photosynthesis: The light reactions*; Ort, D. R., Yocum, C. F., Eds.; Kluwer Academic: Dordrecht, The Netherlands, 1996; pp 137–164.

(4) Kok, B.; Forbush, B.; McGloin, M. *Photochem. Photobiol.* **1970**, *11*, 457–475.

(5) Joliot, P.; Kok, B. In *Bioenergetics of Photosynthesis*; Govindjee, Ed.; Academic Press: New York, 1975; pp 387–412.

(6) It has recently been suggested that Cl^- is not directly involved in the mechanism of oxygen evolution. Olesen et al.⁷ proposed that the role of chloride is to facilitate proton transfer from the Mn cluster to the medium.

(7) Olesen, K.; Andreasson, L. E. *Biochemistry* **2003**, *42*, 2025–2035.

(8) (a) Nield, J.; Orlova, E. V.; Morris, E. P.; Gowen, B.; van Heel, M.; Barber, J. *Nat. Struct. Biol.* **2000**, *7*, 44 (b) Zouni, A.; Witt, H.-T.; Kern, J.; Fromme, P.; Kraub, N.; Saenger, W.; Orth, P. *Nature* **2001**, *409*, 739–743. (c) Kamiya, N.; Shen, J.-R. *Proc. Natl. Acad. Sci. U.S.A.* **2003**, *100*, 98–103.

It has long been known that Ca²⁺ is an essential cofactor for photosynthetic oxygen evolution, given that depletion of Ca²⁺ suppresses oxygen evolving activity.^{1,2} Furthermore, in the absence of Ca²⁺, electron transfer from tyrosine Y_Z to the photooxidized chlorophyll, P₆₈₀⁺, is slowed,¹⁰ and S₂Y_Z^{*} can be trapped^{11,12} with further charge accumulations blocked. Recently, Vrettos et al. proposed that Ca²⁺ acts as a Lewis acid, binding a nucleophilic substrate water in position to attack an electrophilic Mn–O species at the S₄ state.¹³ However, the exact functional role of Ca²⁺ in the OEC remains uncertain. To understand the functional role of Ca²⁺ in the OEC, knowledge of the actual location of the Ca²⁺ binding site of PSII is required. However, Ca²⁺ ions are not located at the present resolution of the X-ray crystal structures.⁸

Other groups have investigated the Ca²⁺ binding site by substitution of Ca²⁺ with other metal ions, motivated by general lack of spectroscopic features of Ca²⁺.^{14–16} Aside from Ca²⁺ itself, of all di- and trivalent metal ions, only Sr²⁺ provides partial restoration of oxygen evolution in Ca²⁺-depleted PSII preparations.^{17,18} Substitution of Sr²⁺ for Ca²⁺ results in a slowing of the S-states transitions,¹⁰ which is consistent with the results of time-resolved EPR experiments monitoring the kinetics of reduction of Y_Z^{*} by the Mn cluster.¹⁹ Sr²⁺ reconstitution also results in a modification of the S₂ state EPR spectrum of the Mn cluster, which suggests that the Ca²⁺ binding site is close to the Mn cluster.^{11,18,20–21} A recent ¹¹³Cd NMR study of Cd²⁺-inhibited PSII preparations suggests that the Ca²⁺ binding site is composed of a symmetric array of ligands including oxygen and chlorine or nitrogen atoms and may be close to the Mn cluster.¹⁶ A number of EXAFS experiments have targeted the Ca²⁺ site and the question of its possible proximity to the Mn cluster.^{22–26} Latimer et al.²³ reported that the Ca²⁺ site is at a 3.5 Å distance from the Mn cluster based on Mn EXAFS experiments on Sr²⁺-reconstituted PSII membranes. This work has been confirmed using strontium EXAFS²⁵ and calcium

EXAFS.²⁶ However, this conclusion has been disputed in another Mn EXAFS study which found no Ca²⁺ within the vicinity (4 Å) of the Mn cluster.²⁴ Given that some EXAFS results are inconsistent, and that the crystal structures of PSII do not resolve the calcium binding site, the question of whether the essential Ca²⁺ is bound close to the OEC Mn cluster remains open.

To help answer this question, we have performed ⁸⁷Sr three-pulse electron spin-echo envelope modulation (ESEEM) experiments. To our knowledge, this is the first use of ESEEM to detect the $I = 9/2$ ⁸⁷Sr nucleus. ESEEM spectroscopy^{27,28} detects magnetic nuclei coupled to the unpaired electrons of a paramagnetic center and is an excellent tool to probe the local structure of a protein in the vicinity of a paramagnetic probe.^{29,30} ESEEM spectroscopy has been extensively exploited to assign the interaction of amino acid residues with the Mn cluster³¹ and to study alcohol and acetate binding at the OEC of the PSII.^{32,33} The Fourier transform of an ESEEM time domain spectrum from a weakly coupled nucleus shows a fundamental peak at the nuclear Larmor frequency, which determines the source of the modulation. Simulation of the time domain ESEEM provides the distance between the paramagnetic species and weakly coupled nuclei through determination of the distance-dependent dipolar coupling.

In this work, we provide positive results of the first ESEEM test of whether the Ca²⁺ binding site is close to the Mn cluster. We use natural abundance Sr and enriched ⁸⁷Sr to reconstitute Ca²⁺-depleted PSII membranes. 93% of natural abundance Sr consists of the $I = 0$ nonmagnetic ⁸⁶Sr and ⁸⁸Sr isotopes. However, the remaining 7% consists of the magnetic $I = 9/2$ ⁸⁷Sr isotope.³⁴ In the absence of the quadrupole interaction, the ESEEM signal scales dramatically with the spin I of the nucleus, with the modulation depth of the time domain ESEEM proportional to $I(I + 1)$. Thus the $I = 9/2$ ⁸⁷Sr nucleus could give a signal 33 times greater than an equivalent $I = 1/2$ proton in the ideal circumstance. In the limit of weak, dipolar hyperfine coupling, the ESEEM modulation scales steeply ($1/r^6$) with the electron–nuclear distance r , and thus our identification of ⁸⁷Sr modulation associated with the S₂ state Mn EPR signal provides a confirmation of a close Mn–Sr interaction. Simulation of the modulation depth provides an independent measure of the Mn–Sr distance.

In addition to the experimental ESEEM results, we use the density functional theory to gain insight into the role of the

- (9) Peloquin, J. M.; Campbell, K. A.; Randall, D. W.; Evanchik, M. A.; Pecoraro, V. L.; Armstrong, W. H.; Britt, R. D. *J. Am. Chem. Soc.* **2000**, *122*, 10926–10942.
- (10) Boussac, A.; Setif, P.; Rutherford, A. W. *Biochemistry* **1992**, *31*, 1224–1234.
- (11) Boussac, A.; Zimmermann, J.-L.; Rutherford, A. W. *Biochemistry* **1989**, *28*, 8984–8989.
- (12) (a) Gilchrist, M. L.; Ball, J. A.; Randall, D. W.; Britt, R. D. *Proc. Natl. Acad. Sci. U.S.A.* **1995**, *92*, 9545–9549. (b) Tang, X.-S.; Randall, D. W.; Force, D. A.; Diner, B. A.; Britt, R. D. *J. Am. Chem. Soc.* **1996**, *118*, 7638–7639.
- (13) Vrettos, J. S.; Stone, D. A.; Brudvig, G. W. *Biochemistry* **2001**, *40*, 7937–7945.
- (14) Bakau, A.; Buser, C.; Dandulakis, G.; Brudvig, G.; Ghanotakis, D. *Biochim. Biophys. Acta* **1992**, *1099*, 131–136.
- (15) Booth, P. J.; Rutherford, A. W.; Boussac, A. *Biochim. Biophys. Acta* **1996**, *1272*, 127–134.
- (16) Matysik, J.; Alia; Nachtegaal, G.; van Gorkom, H. J.; Hoff, A. J.; de Groot, H. J. M. *Biochemistry* **2000**, *39*, 6751–6755.
- (17) Ghanotakis, D. F.; Babcock, G. T.; Yocum, C. F. *FEBS Lett.* **1984**, *167*, 127–130.
- (18) Boussac, A.; Rutherford, A. W. *Biochemistry* **1988**, *27*, 3476–3483.
- (19) Westphal, K. L.; Lydakis-Simantiris, N.; Cukier, R. I.; Babcock, G. T. *Biochemistry* **2000**, *39*, 16220–16229.
- (20) Sivaraja, M.; Tso, J.; Dismukes, G. C. *Biochemistry* **1989**, *28*, 9459–9464.
- (21) Tso, J.; Sivaraja, M.; Dismukes, G. C. *Biochemistry* **1991**, *30*, 4734–4739.
- (22) Yachandra, V. K.; Latimer, M. J.; Derose, V. J.; Mukerji, I.; Sauer, K.; Klein, M. P. *Science* **1993**, *260*, 675–679.
- (23) Latimer, M. J.; Derose, V. J.; Mukerji, I.; Yachandra, V. K.; Sauer, K.; Klein, M. P. *Biochemistry* **1995**, *34*, 10898–10909.
- (24) Riggs-Gelasco, P. J.; Mei, R.; Ghanotakis, D. F.; Yocum, C. F.; Penner-Hahn, J. E. *J. Am. Chem. Soc.* **1996**, *118*, 2400–2410.
- (25) Cinco, R. M.; Robblee, J. H.; Rompel, A.; Fernandez, C.; Yachandra, V. K.; Sauer, K.; Klein, M. P. *J. Phys. Chem. B* **1998**, *102*, 8248–8256.
- (26) Cinco, R. M.; Holman, K. L. M.; Robblee, J. H.; Yano, J.; Pizarro, S. A.; Bellacchio, E.; Sauer, K.; Yachandra, V. K. *Biochemistry* **2002**, *41*, 12928–12933.

- (27) Kevan, L. In *Time Domain Electron Spin Resonance*; Kevan, L., Schwartz, R. N., Eds.; Wiley and Sons: New York, 1979; pp 280–341.
- (28) Dikanov, S. A.; Tsvetkov, Y. D. *Electron Spin–Echo Envelope Modulation Spectroscopy*; CRC Press: 1992; pp 303–357.
- (29) Mims, W. B.; Davis, J. L.; Peisach, J. *J. Magn. Reson.* **1990**, *86*, 273–292.
- (30) (a) Britt, R. D. In *Biophysical Techniques in Photosynthesis*; Ames, J., Hoff, A. J., Eds.; Kluwer Academic: Dordrecht, The Netherlands, 1996; pp 235–253. (b) Britt, R. D. In *Paramagnetic Resonance of Metallobiomolecules*; Telsner, J., Ed.; ACS Symposium Series; American Chemical Society: Washington, DC, 2003; pp 16–54.
- (31) (a) Debus, R. J.; Campbell, K. A.; Gregor, W.; Li, Z. L.; Bumap, R. L.; Britt, R. D. *Biochemistry* **2001**, *40*, 3690–3699. (b) Debus, R. J.; Campbell, K. A.; Peloquin, J. M.; Pham, D. P.; Britt, R. D. *Biochemistry* **2000**, *39*, 470–478. (c) Tang, X. S.; Diner, B. A.; Larsen, B. S.; Gilchrist, M. L.; Lorigan, G. A.; Britt, R. D. *Proc. Natl. Acad. Sci. U.S.A.* **1994**, *91*, 704–709.
- (32) Force, D. A.; Randall, D. W.; Lorigan, G. A.; Clemens, K. L.; Britt, R. D. *J. Am. Chem. Soc.* **1998**, *120*, 13321–13333.
- (33) Clemens, K. L.; Force, D. A.; Britt, R. D. *J. Am. Chem. Soc.* **2002**, *124*, 10921–10933.
- (34) We note here that a ⁴³Ca ESEEM experiment would be expected to give better results, since the magnetogyric ratio of ⁴³Ca is larger. Unfortunately, this isotope is also extremely expensive.

structural environment of the $\text{Ca}^{2+}/\text{Sr}^{2+}$ in the protein on the quadrupolar parameters of the metal ion. Recently we have shown that, although the quantum chemical calculations are not able to reproduce the absolute magnitudes of the quadrupolar couplings with a high accuracy at the reasonable computational costs, they can be successfully used to monitor the trends and explain the changes in the quadrupolar parameters values related to the conformational changes in the vicinity of the nuclei in various molecular systems.³⁵ The goal of the calculations presented here is to estimate an order of magnitude of the quadrupolar interaction in various protein sites exhibiting different $\text{Ca}^{2+}/\text{Sr}^{2+}$ coordination environments, and thus gain information about possible configurations of the ligands to the $\text{Ca}^{2+}/\text{Sr}^{2+}$ ion.

Materials and Methods

Sample Preparation. PSII membranes were prepared from spinach based on the procedure developed by Berthold, Babcock, and Yocum^{36,37} with specific details provided by Campbell et al.³⁸ These PSII samples were stored at $-20\text{ }^{\circ}\text{C}$ in 0.3 M sucrose, 30 mM NaCl, 25 mM MES, and 5 mM MgCl_2 , pH 6.5 at approximately 4 mg of Chl/mL before use. Ca^{2+} -depletion treatment was performed according to the NaCl washing procedure of Boussac and Rutherford.¹⁸ Briefly, NaCl washing of PSII membranes was done under room light at $4\text{ }^{\circ}\text{C}$ at 0.5 mg of Chl/mL in 0.3 M sucrose, 1.2 M NaCl, and 25 mM MES, pH 6.5. After a 30 min incubation, 100 μM EGTA was added, and the NaCl washed PSII membranes were pelleted by 15 min centrifugation at 17 000 rpm, washed once in 30 mM NaCl, 25 mM MES, pH 6.5, and 100 μM EGTA, and pelleted again by 15 min centrifugation at 17 000 rpm. These calcium-depleted PSII membranes were then resuspended in 25 mM MES, 30 mM NaCl, and either 20 mM SrCO_3 for Sr^{2+} -reconstituted samples or 20 mM CaCl_2 for Ca^{2+} -reconstituted samples and homogenized slowly under room light for 4 min. These samples were then pelleted by centrifugation at 17 000 rpm for 20 min. These pellets were resuspended with buffers containing either SrCO_3 or CaCl_2 in the dark and were pelleted for 30 min at 17 000 rpm. Sucrose was omitted to prevent Ca^{2+} contamination and to speed up metal reconstitution. The samples were loaded in calibrated quartz EPR tubes and, after 30–50 min of dark adaptation, frozen and stored at 77 K. 92.6% enriched $^{87}\text{SrCO}_3$ was purchased from Cambridge Isotope Laboratories and used as received.³⁹ The samples were illuminated for 5 min at 195 K for the “light” S_2 -state spectra.

EPR Spectroscopy. CW-EPR spectra were collected at a temperature of 7 K with a Bruker ECS106 X-band CW-EPR spectrometer equipped with an Oxford ESR900 liquid helium cryostat and an ITC503 temperature controller. ESEEM spectra were collected at a temperature of 4.2 K with a laboratory-built pulsed EPR spectrometer.⁴⁰ Three-pulse time domain ESEEM experiments were performed by incrementing T in the stimulated echo sequence: $\pi/2 - \tau - \pi/2 - T - \pi/2 -$ stimulated echo. A cosine Fourier backfill procedure was used to reconstruct the instrumental dead time for all three-pulse data in order to generate the final displayed Fourier transforms.⁴¹ The EPR spectra were collected for both dark and illuminated samples; the “dark”

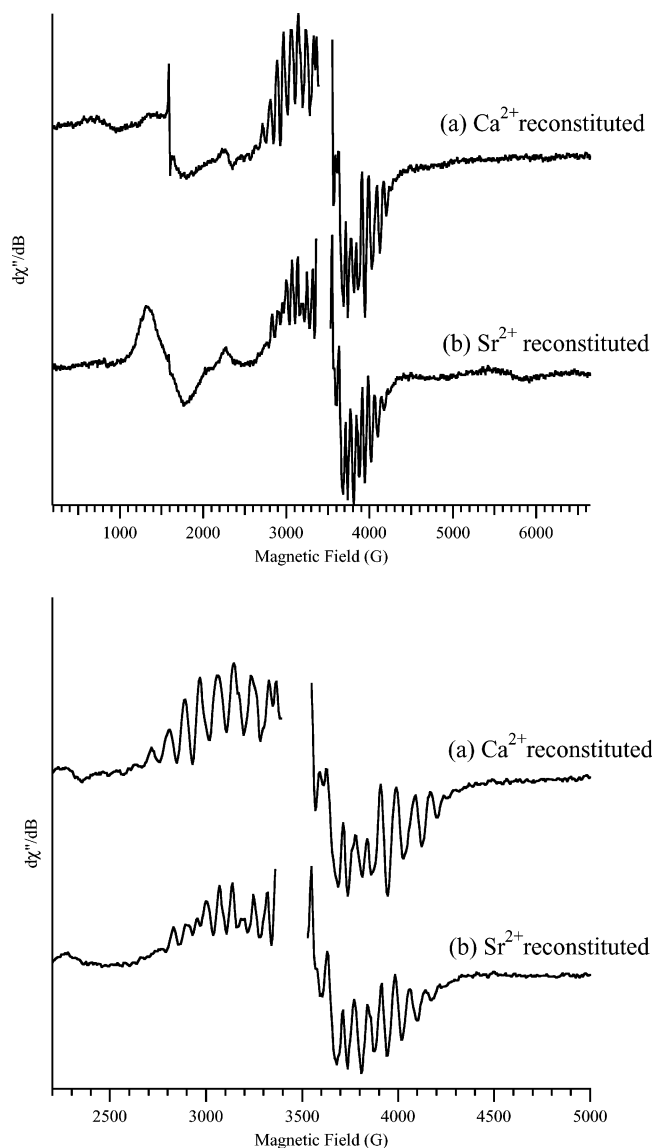


Figure 1. CW-EPR spectra of (a) Ca^{2+} - and (b) Sr^{2+} -reconstituted PSII samples after 1.2 M NaCl treatment. Spectra are the difference between spectra from illuminated and dark-adapted samples (top). Closeup of the $g = 2$ multiline signal region (bottom). Instrument parameters: temperature, 7.0 K; microwave frequency, 9.68 GHz; microwave power, 3.2 mW; modulation amplitude, 16 G; modulation frequency, 100 kHz.

background spectra were subtracted from the “light” S_2 -state spectra to produce the “light minus dark” difference spectra isolating the changes produced upon forming the S_2 -state via the illumination. ESEEM simulations were performed using a numerical matrix diagonalization procedure. The simulation code was kindly provided by Professor Kurt Warncke.

DFT Calculations. The DFT calculations of the electric field gradient were carried out using the Gaussian 98 package⁴² with the

(35) Kim, S. H.; Aznar, C.; Brynda, M.; Silks, L. A. P.; Michalczyk, R.; Unkefer, C. J.; Woodruff, W. H.; Britt, R. D. *J. Am. Chem. Soc.* **2004**, *126*, 2328–2338.

(36) Berthold, D. A.; Babcock, G. T.; Yocum, C. F. *FEBS Lett.* **1981**, *134*, 231–234.

(37) Ford, R. C.; Evans, M. C. W. *FEBS Lett.* **1983**, *160*, 159–164.

(38) Campbell, K. A.; Gregor, W.; Pham, D. P.; Peloquin, J. M.; Debus, R. J.; Britt, R. D. *Biochemistry* **1998**, *37*, 5039–5045.

(39) $^{87}\text{SrCO}_3$ is the only chemical form commercially available for the ^{87}Sr isotope. In preliminary CW-EPR experiments, to check the effect of carbonate on the S_2 multiline, we observed no differences in the multiline signals of SrCO_3 - and SrCl_2 -treated samples. The formation of the altered Mn multiline signal shows that, despite limited solubility of SrCO_3 , we are obtaining adequate Sr^{2+} concentration in the resuspension buffer to generate this S_2 state signal.

(40) Sturgeon, B. E.; Britt, R. D. *Rev. Sci. Instrum.* **1992**, *63*, 2187–2192.

(41) Mims, W. B. *J. Magn. Reson.* **1984**, *59*, 291–306.

(42) Frisch, M. J.; Trucks, G. W.; Schlegel, H. B.; Scuseria, G. E.; Robb, M. A.; Cheeseman, J. R.; Zakrzewski, V. G.; Montgomery, J. A., Jr.; Stratmann, R. E.; Burant, J. C.; Dapprich, S.; Millam, J. M.; Daniels, A. D.; Kudin, K. N.; Strain, M. C.; Farkas, O.; Tomasi, J.; Barone, V.; Cossi, M.; Cammi, R.; Mennucci, B.; Pomeli, C.; Adamo, C.; Clifford, S.; Ochterski, J.; Petersson, G. A.; Ayala, P. Y.; Cui, Q.; Morokuma, K.; Malick, D. K.; Rabuck, A. D.; Raghavachari, K.; Foresman, J. B.; Ciolowski, J.; Ortiz, J. V.; Baboul, A. G.; Stefanov, B. B.; Liu, G.; Liashenko, A.; Piskorz, P.; Komaromi, I.; Gomperts, R.; Martin, R. L.; Fox, D. J.; Keith, T.; Al-Laham, M. A.; Peng, C. Y.; Nanayakkara, A.; Gonzalez, C.; Challacombe, M.; Gill, P. M. W.; Johnson, B.; Chen, W.; Wong, M. W.; Andres, J. L.; Head-Gordon, M.; Replogle, E. S.; Pople, J. A. *Gaussian 98*, revision A.7. Gaussian, Inc.: Pittsburgh, PA, 1998.

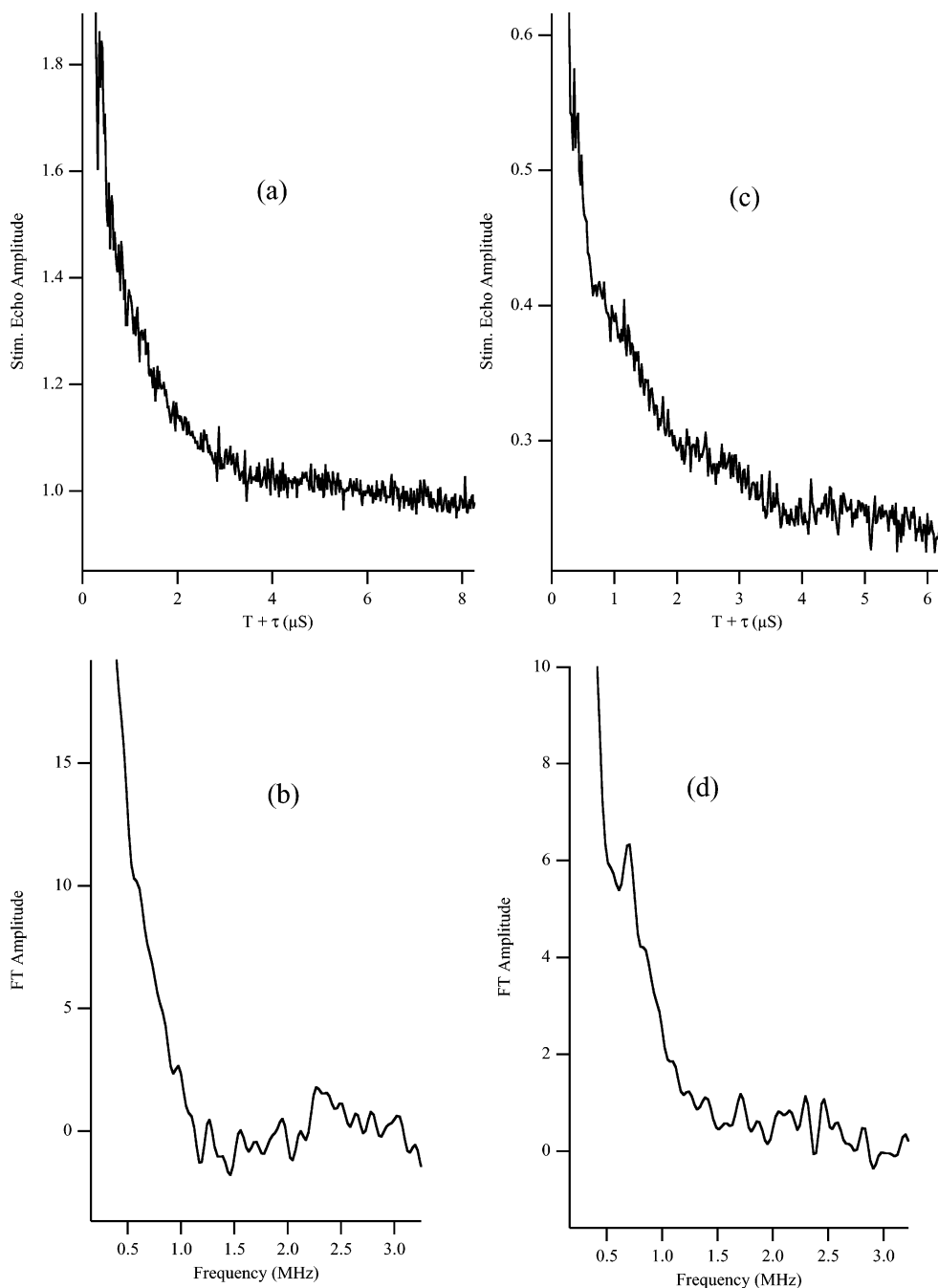


Figure 2. Time domain (a, c) and Fourier transform (b, d) three-pulse ESEEM spectra of natural abundance Sr-reconstituted (a, b) and enriched ^{87}Sr -reconstituted (c, d) PSII samples. Instrument parameters: microwave frequency, 9.334 GHz; microwave power, 50 W; magnetic field, 3436 G; interpulse time τ , 205 ns; starting T , 75 ns; T -increment, 20 ns; $\pi/2$ pulse, 15 ns; repetition rate, 200 Hz; temperature, 4.2 K.

hybrid B3LYP functional in gaseous phase. For all the calculations, a 6-31g* basis set was used, except for the strontium atom where a smaller 3-21g* basis set was used. The representations of the molecular structures were generated with the MOLEKEL program.⁴³ The traceless electric field gradient (EFG) tensor elements are related to the quadrupolar coupling constant e^2qQ by

$$e^2qQ = e^2Q \langle q_{zz} \rangle / h$$

To convert the q_{zz} output from atomic units (au) into the ^{3}Ca quadrupolar coupling constant, a value of $e^2Q/h = -9.66$ MHz was used. This corresponds to a ^{43}Ca quadrupolar moment $Q = -0.0408$

$\times 10^{-24}$ cm².⁴⁴ For ^{87}Sr , a value of $e^2Q/h = 79.40$ MHz was used, corresponding to a ^{87}Sr quadrupolar moment $Q = 0.335 \times 10^{-24}$ cm².⁴⁴

Results

CW-EPR Spectroscopy. Figure 1 shows the CW-EPR spectra of Ca^{2+} -reconstituted (a) and Sr^{2+} -reconstituted (b) PSII membranes. The upper panel shows the full field range of the signals, whereas the lower panel focuses on the $g = 2$ multiline region. Each spectrum is the difference between the spectrum recorded after 195 K illumination (S_2 -state) and the preillumination.

(43) MOLEKEL 4.3. Flukiger, P.; Luthi, H. P.; Portmann, S.; Weber, J. Swiss Center for Scientific Computing: Manno, Switzerland, 2000–2002.

(44) (a) Lide, D. R., Ed. *Handbook of Chemistry and Physics*, 79th ed.; CRC Press: Boca Raton, FL, 1998. (b) Larsen, F. H.; Skibsted, J.; Jakobsen, H. J.; Nielsen, N. C. *J. Am. Chem. Soc.* **2000**, *122*, 7080–7086.

nation spectrum of the dark adapted (S_1 -state) sample. The Ca^{2+} -reconstituted spectrum shows very little of the $g = 4.1$ signal, while the Sr^{2+} -reconstituted sample has a significant increase in the amplitude of this higher spin state Mn EPR signal. The multiline signal for the Ca^{2+} -reconstituted sample is almost identical to that of the control PSII sample (not shown). The Sr^{2+} -reconstituted samples show an altered multiline signal, which has much narrower hyperfine splittings and a different intensity pattern when compared to that of control samples (see lower panel, Figure 1).¹⁸ The modification of the multiline signal induced by Sr is similar to those induced by NH_3 binding.⁴⁵ For NH_3 , such a spectral change was considered as evidence that NH_3 binds directly to the Mn cluster in the substrate site.⁴⁶ Similar spectral changes have been reported on Sr^{2+} -reconstituted samples following depletion of Ca^{2+} using a high concentration of NaCl .¹⁸ These CW-EPR spectra demonstrate that we have successfully replaced Ca^{2+} with Sr^{2+} . We note that the characteristic $S_2Y_Z^*$ split EPR signal was also observed in the Ca^{2+} -depleted samples when illuminated at 0°C for 2 min (data not shown). The presence of the split signal shows that Ca^{2+} is removed from its cofactor binding site before reconstitution with Sr^{2+} or Ca^{2+} .

ESEEM Spectroscopy. Three-pulse ^{87}Sr ESEEM provides an excellent method for probing the Mn cluster–Sr(Ca) distance. Three-pulse ESEEM is preferred over two-pulse ESEEM for this study, since the three-pulse stimulated echo decays with the longer T_1 relaxation rather than the short T_2 phase memory time that rapidly damps the two-pulse echo pattern. This facilitates observation of multiple cycles of low-frequency modulations from low γ nuclei such as ^{87}Sr . The ^{87}Sr Larmor frequency is only around 600 kHz for typical magnetic fields near $g = 2$ for X-band EPR experiments.

Figure 2 shows three-pulse ESEEM results obtained from the Sr^{2+} -reconstituted samples with either natural abundance Sr or enriched ^{87}Sr . Generally, for the best results and for the simplicity of interpretation, three-pulse ESEEM experiments targeting weakly coupled nuclei should be performed with τ set equal to one-half of the free nuclear precession period. In this case, the modulation amplitude factor $\sin^2(\omega\tau/2)$ in eq 2 (*vide infra*) equals 1, which allows for full ESEEM modulation depth. However, because of the short phase memory of the multiline signal of the Sr^{2+} -reconstituted sample, we could not use the very long $\tau = 786$ ns value corresponding to $1/2$ the ^{87}Sr modulation period. The ESEEM spectra were instead obtained at a $\tau = 205$ ns, a relatively short τ value which is specifically chosen to eliminate proton modulation. The $\tau = 205$ ns value used here results in the factor $\sin^2(\omega\tau/2)$ equaling only 0.16. Thus the combination of the low Larmor frequency for ^{87}Sr and the short phase memory of the multiline signal constrains the sensitivity of the three-pulse ESEEM experiment to a small fraction of the ideal case.

The time domain three-pulse ESEEM spectrum using natural abundance Sr exhibits no modulation by ^{87}Sr (Figure 2a). There is also no observable strontium peak at 0.64 MHz, the ^{87}Sr Larmor frequency, in the corresponding Fourier Transform spectrum (Figure 2b), which is not surprising given that only 7% of the natural abundance Sr is the magnetic ^{87}Sr isotope.

On the other hand, the time domain three-pulse ESEEM of the ^{87}Sr -enriched reconstituted sample clearly exhibits modulation arising from weakly coupled ^{87}Sr , with a period of 1567 ns corresponding to the inverse of the 0.64 MHz ^{87}Sr Larmor frequency (Figure 2c). A 0.64 MHz peak assignable to ^{87}Sr is also evident in the Fourier transform spectrum (Figure 2d). The ESEEM spectra shown in Figure 2 show a clear difference between the two pairs of samples, which differ only in the enrichment of one sample with the magnetic ^{87}Sr isotope over the small (7%) amount present in the other. Moreover, the modulation introduced by ^{87}Sr enrichment occurs at the ^{87}Sr Larmor frequency (0.64 MHz at 3436 G). These ESEEM differences and the ^{87}Sr frequency were reproduced in an independent set of ^{87}Sr and natural abundance Sr samples (data not shown). These results clearly demonstrate that our Ca^{2+} -depletion and Sr^{2+} -repletion procedure introduces ^{87}Sr into the immediate vicinity of the Mn cluster (giving rise to the Sr-altered multiline EPR signal). The peak at 0.64 MHz shows no clear sign of any nuclear-quadrupole-induced splitting, probably because of a nearly cubic electronic environment for the closed shell Sr^{2+} ion. We explore a range of possible Mn–Sr distances and further discuss quadrupolar interactions in the discussion section.

Discussion

This discussion section is organized in several tiers. We start with a purely analytical approach to the ESEEM analysis, assuming a simple point dipole approximation for the electron spin and ignoring the nuclear quadrupolar interaction for the $I = 9/2$ ^{87}Sr nucleus. We then add the effects of nonzero quadrupolar interaction through numerical simulation. This leads to a DFT calculational section exploring what range of e^2qQ values are expected for different ^{87}Sr (and ^{43}Ca) environments. Finally we include a section of modeling the Mn–Sr/Ca distance in terms of magnetic and structural models for the S_2 -state Mn cluster.

(1) Analytical Approach. Dikanov et al.⁴⁷ derived analytical expressions for the modulation effects in three-pulse ESEEM resulting from the hyperfine interaction between an $S = 1/2$ electron and a nucleus with an arbitrary spin I in the absence of nuclear quadrupolar interactions.

For a nucleus with $I = 9/2$, such as ^{87}Sr , in the absence of quadrupolar effects, the stimulated echo modulation function for the $S = 1/2$, $I = 9/2$ spin system can be written as

$$V_{\text{mod}}^{9/2} = \frac{1}{2} \left\{ \frac{1}{2I+1} \sum_{m=-9/2}^{m=9/2} \cos m\xi^\alpha + \frac{1}{2I+1} \sum_{m=-9/2}^{m=9/2} \cos m\xi^\beta \right\} = \frac{1}{2} \left\{ 51.2 \left(\cos^9 \frac{\xi^\alpha}{2} + \cos^9 \frac{\xi^\beta}{2} \right) - 102.4 \left(\cos^7 \frac{\xi^\alpha}{2} + \cos^7 \frac{\xi^\beta}{2} \right) + 67.2 \left(\cos^5 \frac{\xi^\alpha}{2} + \cos^5 \frac{\xi^\beta}{2} \right) - 16 \left(\cos^3 \frac{\xi^\alpha}{2} + \cos^3 \frac{\xi^\beta}{2} \right) + \left(\cos \frac{\xi^\alpha}{2} + \cos \frac{\xi^\beta}{2} \right) \right\} \quad (1)$$

where

(45) Beck, W. F.; de Paula, J. C.; Brudvig, G. W. *J. Am. Chem. Soc.* **1986**, *108*, 4018–4022.

(46) Britt, R. D.; Zimmermann, J.-L.; Sauer, K.; Klein, M. P. *J. Am. Chem. Soc.* **1989**, *111*, 3522–3532.

(47) Dikanov, S. A.; Shubin, A. A.; Parmon, V. N. *J. Magn. Reson.* **1981**, *42*, 474–487.

$$\cos\left(\frac{\xi^\alpha}{2}\right) = 1 - 2K \sin^2 \frac{\omega_\alpha(\tau + T)}{2} \sin^2 \frac{\omega_\beta\tau}{2}$$

$$\cos\left(\frac{\xi^\beta}{2}\right) = 1 - 2K \sin^2 \frac{\omega_\beta(\tau + T)}{2} \sin^2 \frac{\omega_\alpha\tau}{2} \quad (2)$$

$$K = \left(\frac{\omega_1 B}{\omega_\alpha \omega_\beta}\right)^2, \quad \omega_1 = \frac{g_1 \beta_1 H_0}{\hbar} \quad (3)$$

$$\omega_\alpha = \left[\left(\frac{A}{2} + \omega_1\right)^2 + \left(\frac{B}{2}\right)^{2\frac{1}{2}}\right] \quad (4)$$

$$\omega_\beta = \left[\left(\frac{A}{2} - \omega_1\right)^2 + \left(\frac{B}{2}\right)^{2\frac{1}{2}}\right] \quad (5)$$

$$A = T(3 \cos^2 \theta - 1), \quad B = 3T \sin \theta \cos \theta$$

$$T = \frac{g g_1 \beta \beta_1}{\hbar r^3} \quad (6)$$

In these expressions, g and g_1 are the electronic and nuclear g factors, β and β_1 are the Bohr magneton for an electron and a nucleus, H_0 is the magnitude of the applied magnetic field, θ is the angle between the magnetic field vector and the vector connecting the electron and the nucleus, and r is the distance between the electron and the nucleus, approximating the electron spin as a point dipole. In the limit of relatively weak dipolar-dominated couplings ($A \approx 0$, $T < \omega_1$ and $\omega_\alpha \approx \omega_\beta \approx \omega$), the modulation depth parameter K can be written approximately as

$$K = \left(\frac{B}{\omega}\right)^2 = \left(\frac{9}{4}\right) \left(\frac{g\beta}{H_0}\right)^2 \frac{\sin^2(2\theta)}{r^6} \quad (7)$$

This equation can be modified by averaging over a sphere to account for all of the possible orientations of the electron–nucleus position vector with respect to the magnetic field:

$$K = \left(\frac{6}{5}\right) \left(\frac{g\beta}{H_0 r^3}\right)^2 \quad (8)$$

We note there is no appreciable “orientation selection”⁴⁸ for X band ESEEM of the relatively isotropic multiline EPR signal.

In addition, the factors $\sin^2 \omega_\beta\tau/2 \approx \sin^2 \omega_\alpha\tau/2 \approx \sin^2 \omega\tau/2$ correspond to a value of 0.16 at the experimental magnetic field, 3436 G, and τ value, 205 ns.

The above $V_{\text{mod}}^{9/2}$ equation can be used to calculate the distance between the ^{87}Sr nucleus and the unpaired electron in a point dipole limit, once a correction is made for the decay. A decay factor must be included to account for the echo decay observed in the time domain. Since a pure single-exponential function does not fit well with the echo decay, we rather have used the function: $A + B \exp(-(\tau + T)/t)$, where t is an empirical echo decay time (best fit $t = 1.23 \mu\text{s}$). Thus we can obtain the distance, r , by fitting the time domain of three-pulse ESEEM.

Figure 3 shows a trace (dotted line) using the above equation with $r = 4.5 \text{ \AA}$. Since we neglect the quadrupolar effect for this simulation, some error may be introduced; an effect of a nonzero quadrupolar interaction for the ^{87}Sr nucleus could be

to damp or dephase the fundamental ω_1 modulation component at longer interpulse times (T) (*vide infra*).⁴⁹

(2) Numerical Simulation. To support this analytical calculation and to expand to the nonzero quadrupolar interaction case, we performed simulations of three-pulse ESEEM data using a numerical matrix diagonalization procedure. A simulation of the three-pulse ESEEM was performed using the parameters $A_{\text{iso}} = 0 \text{ MHz}$ and $A_{\text{dip}} = 0.038 \text{ MHz}$, which corresponds to $r = 4.5 \text{ \AA}$ (solid line in Figure 3). The simulation was multiplied by the same exponential decay function as that used for the analytical expression. We obtained a good agreement between the simulation and the analytical expression results. However, this initial simulation was performed without using a quadrupole interaction.

In general, for an $I > 1/2$ nucleus such as ^{87}Sr , we need to consider the effects of quadrupolar interactions on the ESEEM spectra. To observe how a quadrupolar interaction can affect the modulation of the time domain of ESEEM spectra, we performed simulations over a range of values of the quadrupolar parameters e^2qQ and η . The results of one set of simulations, $0 \leq e^2qQ \leq 4 \text{ MHz}$, $\eta = 0.2$, is shown in Figure 4. (For this figure, the simulated time domain is not multiplied by any decay function in order to emphasize the full time range of quadrupolar effects on the predicted spectra.)

Small e^2qQ values (1 MHz or less) lead to greater damping of the time domain signal but do not result in FFT peak frequency shifts or splittings. However, as seen in Figure 4, e^2qQ values greater than 1 MHz reduce the modulation depth relative to the zero quadrupole case, and for large e^2qQ values, one observes appreciable shifts in the FFT peak frequency. With even higher values, one observes increased complexity in the time domain modulation patterns with significant decreased modulation, which leads to added frequency components with smaller amplitude in the FFT frequency domain (data not shown). Varying η over its 0–1 range for a fixed e^2qQ value leads to frequency shifts but little change in modulation depth.

The observation that echo modulation depth decreases with larger quadrupole interaction was discussed by Rowan,⁵⁰ who showed that when the quadrupole interaction is much stronger than the electron nuclear hyperfine interaction, the nuclear spin quantum axis is determined by the direction of the quadrupole interaction and is not changed appreciably by electron spin flips induced by the microwave pulses. Therefore there is little nuclear spin state coherent superposition induced by the microwave pulse and therefore little echo envelope modulation results.

Noting some tradeoff between the effects of varying e^2qQ and η in the simulations, we consider that a maximum e^2qQ value of approximately 5 MHz is consistent with the observed modulation depth and the close match of the experimental frequency to the 0.64 MHz ^{87}Sr larmor frequency. We note that even for modest e^2qQ values, the effect of the quadrupolar couplings is to reduce the modulation depth, so the zero quadrupolar calculated point dipole distance of 4.5 \AA should be taken as an upper limit in the simulations.

(3) DFT Calculations on the Nuclear Quadrupole Interactions in Ca^{2+} and Sr^{2+} Binding Sites in Proteins. One may obtain an estimate from DFT calculations of how large the

(48) Hoffman, B. M.; Derose, V. J.; Doan, P. E.; Gurbiel, R. J.; Houseman, A. L. P.; Tesler, J. In *Biological Magnetic Resonance*; Berliner, L. J., Reuben, J., Eds.; Plenum Press: New York, 1993; pp 151–218.

(49) Shubin, A. A.; Dikanov, S. A. *J. Magn. Reson.* **1983**, *52*, 1–12.

(50) Rowan, L. G. *J. Magn. Reson.* **1987**, *74*, 308–315.

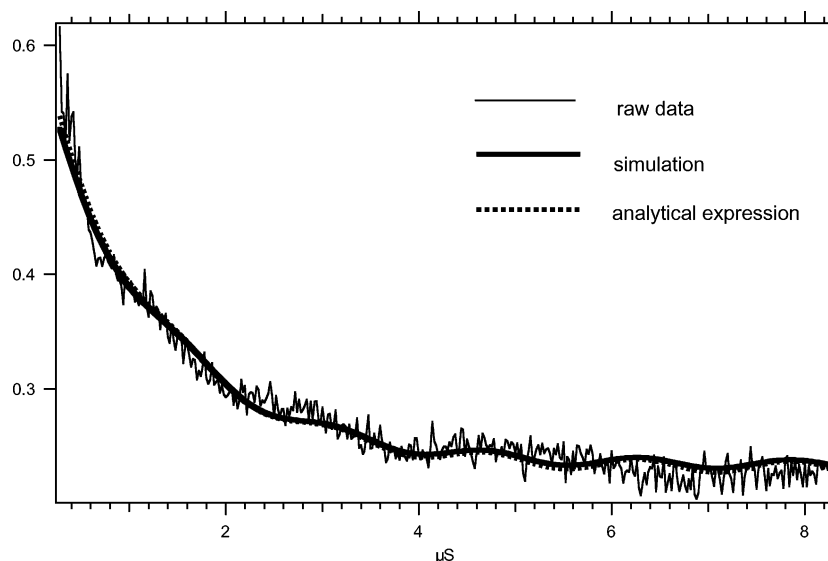


Figure 3. Curve fit of the three-pulse ESEEM time domain of the ^{87}Sr -reconstituted PSII sample with $r = 4.5 \text{ \AA}$ using the analytical expression (dotted line) and the simulation using matrix diagonalization (solid line). A quadrupolar effect is not included.

nuclear quadrupole coupling effect would be for ^{87}Sr or ^{43}Ca bound in a typical Ca^{2+} -binding site.

As noted in the Introduction, calcium cannot be located in the PSII X-ray structures with the available resolution. Thus, we could not perform the calculation of the X-ray derived coordinates of this particular site and had to adopt another approach, which consists of calculating the quadrupolar interaction for a few available Ca^{2+} sites in various proteins as well as for a model Mn/Ca^{2+} OEC cluster. It is established that Ca^{2+} prefers to bind to “hard” oxygen containing ligands such as carboxylates, carbonyls, water and hydroxyl oxygen atoms. Having this in mind and that the observed coordination number in different calcium binding sites varies from 6 to 8,⁵¹ we targeted calculations for three different protein geometries. Two different Ca^{2+} binding sites from concanavalin A and one Ca^{2+} site from baboon α -lactalbumin were selected from available crystal structures in the Protein Data Bank.⁵² The coordination numbers for these sites are 6 and 8 for concanavalin A and 7 for the α -lactalbumin, respectively (Figure 5). Additionally, we have also performed the EFG calculations on the partially optimized model Ca^{2+} site in the three Mn plus Ca OEC cluster geometry proposed by Siegbahn.⁵³ This computational model, with the addition of a fourth Mn out of the core, provides a nice match to our EPR/ENDOR derived model.⁹

Only a very few papers deal with the quadrupolar coupling of the ^{43}Ca isotope, and e^2qQ values measured by solid state NMR for ^{43}Ca binding sites in proteins are relatively rare. Table 1 presents the calculated values of e^2qQ in the four different protein/model sites together with the available, experimentally determined e^2qQ data for ^{43}Ca from a solid-state NMR studies. The calculated ^{43}Ca e^2qQ values are comparable to the experimentally observed values of quadrupolar coupling in different proteins. The calculated quadrupolar interactions for the three sites extracted from concanavalin A and α -lactalbumin range from 0.53 to 1.54 MHz, which agrees rather well with

the experimental range of 0.75 to 1.79 MHz (except for the values reported for a weak Ca site in PLA2) and suggests that at this step the calculations might be considered as reliable. To the best of our knowledge, the only experimental data available for the quadrupolar coupling of ^{87}Sr were reported by Larsen et al.^{44b} from the solid-state NMR study using a quadrupolar Carr–Purcell–Meiboom–Gill (QCPMG) pulse sequence on $\text{Sr}(\text{NO}_3)_2$ and SrMoO_4 . To first check to what extent the EFG calculations might reasonably reproduce the strontium quadrupolar couplings, we have calculated the ^{87}Sr e^2qQ value for the Sr site in strontium nitrate. The calculated value (21.0 MHz) is slightly bigger than the experimental one (15.4 ± 0.2 MHz) but reflects the correct order of magnitude of the quadrupolar interaction. The calculations performed on the Sr^{2+} -substituted protein sites were then performed in two steps. First, the Ca^{2+} was directly substituted by Sr^{2+} in the model protein sites previously used for the calculation of the ^{43}Ca e^2qQ . In the second step, the selected model sites were fully optimized with the substituted Sr^{2+} ion, and the ^{87}Sr e^2qQ values were recalculated based on the optimized geometries. These calculations result in much bigger values of e^2qQ for ^{87}Sr compared to ^{43}Ca , ranging from 14.5 to 26.0 MHz for the nonoptimized sites to from 31.4 to 39.2 MHz for the optimized structures. In general, larger e^2qQ values are indeed expected for ^{87}Sr compared to ^{43}Ca , since the Q value for ^{87}Sr is almost an order of magnitude bigger than the analogous value for ^{43}Ca , translating to bigger e^2qQ values in the same chemical environment. But then the question remains open: Why do we not observe such large quadrupolar couplings in the experimental spectra of ^{87}Sr -substituted PSII preparations? One possible reason might be that the ^{87}Sr coordinating sphere in the substituted Ca binding site of PSII is very highly symmetric. This is in accordance with the finding by Matysik et al.,¹⁶ who probed the PSII Ca binding site with ^{113}Cd NMR and pointed out that its geometry must be highly symmetric and includes a six-coordinated Ca^{2+} with oxygen and eventually some nitrogen and/or chlorine ligands. To probe the degree of sensitivity of the quadrupolar coupling of the Ca(Sr) ions upon changes in ligand symmetry, we have also performed a series of calculations

(51) Dudev, T.; Lim, C. *Chem. Rev.* **2003**, *103*, 773–787.

(52) Berman, H. M.; Westbrook, J.; Feng, Z.; Gilliland, G.; Bhat, T. N.; Weissig, H.; Shindyalov, I. N.; Bourne, P. E. *The Protein Data Bank, Nucleic Acids Research* **2000**, *28*, 235–242

(53) Siegbahn, P. E. M. *Inorg. Chem.* **2000**, *39*, 2923–2935.

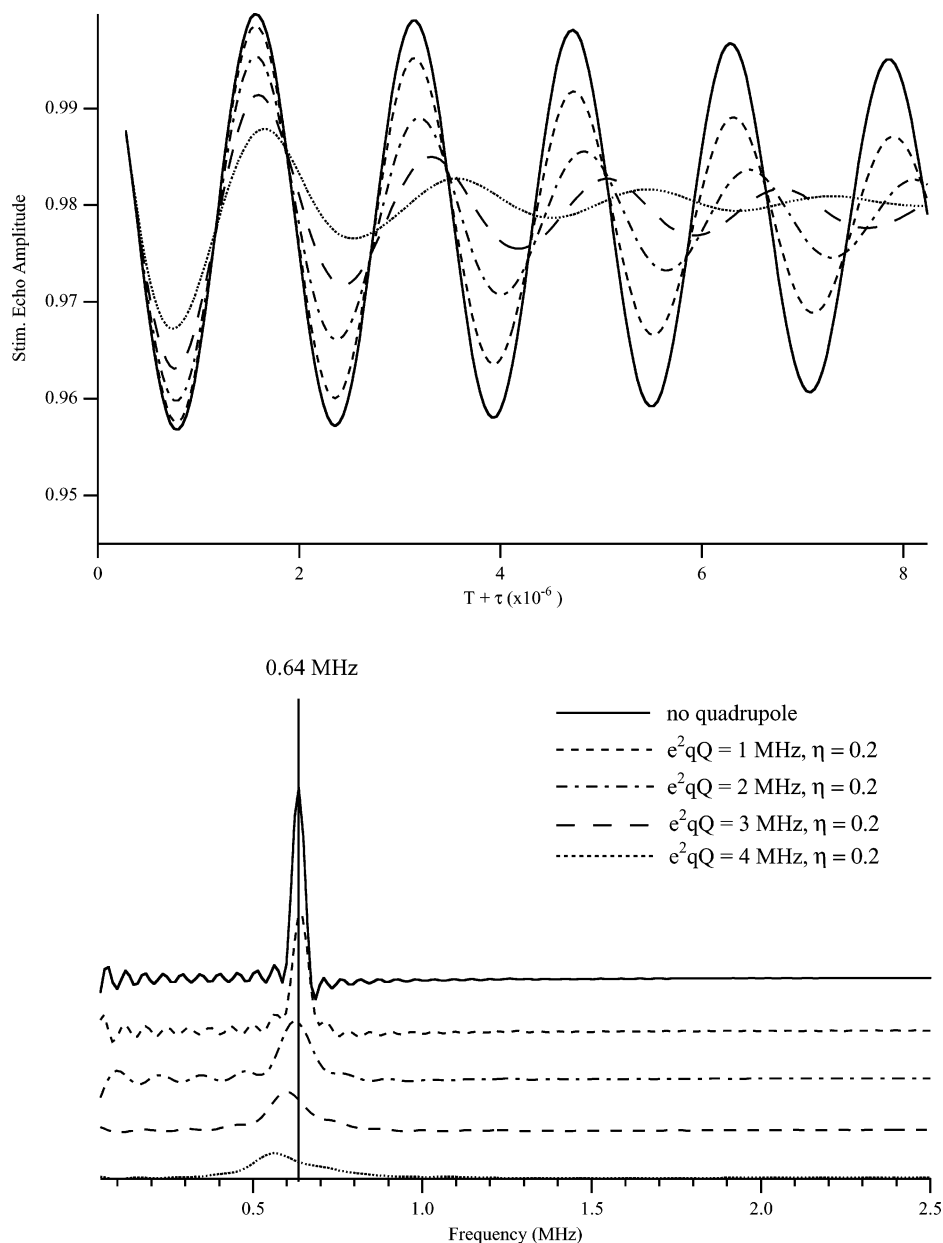


Figure 4. Simulated time domain and frequency domain of three-pulse ESEEM spectra with different e^2qQ values and fixed $\eta = 0.2$. Other parameters are the same as those in Figure 3.

on a model Ca(Sr) site of C_{2h} symmetry with six coordinating oxygen atoms, four of them being waters in equatorial plane and two axial OH groups. Whereas in the case of the $\text{Ca}(\text{H}_2\text{O})_4(\text{OH})_2$ an elongation of the Ca–OH bond by 0.1 Å corresponds to a change of about 0.2 MHz in the e^2qQ values, the analogous geometrical change in the case of the strontium ion induces a difference in quadrupolar coupling of 14.3 MHz. These results indicate that the quadrupolar coupling of the Sr might be considerably affected by the minor modification of the geometry of the surrounding protein. Even considering that this protein exhibits an important degree of rigidity in the surrounding protein, one might expect slight geometrical changes in the coordination sphere of the Ca binding site upon the substitution with the Sr ion.

In conclusion of this DFT calculational section, the calculated range for ^{87}Sr quadrupolar couplings for Sr^{2+} introduced into typical Ca^{2+} protein sites trends appreciably higher than seems

to be supported by this first ^{87}Sr ESEEM experiment. In our experience, DFT calculations of quadrupolar couplings tend to be within about a factor of about 2 of the experimental values, so perhaps the DFT calculations are somewhat overestimating the e^2qQ values for a typical Sr/Ca site. It is also possible that the Sr^{2+} -substituted Ca^{2+} binding site near the OEC provides a very symmetric coordination environment. It is important for us to obtain a more precise measurement of the quadrupolar coupling in future experiments. In particular, work with higher frequency spectrometers will allow us to move the ESEEM/ENDOR frequency of the low γ ^{87}Sr nucleus up to a more favorable frequency range. Also important is to supplement this work with ESEEM targeting of the more expensive ^{43}Ca nucleus, which in comparison to ^{87}Sr has a larger magnetic moment and a much smaller quadrupolar moment.

(4) Tetranuclear Model. In addition to the complications of nonzero quadrupolar couplings, the 4.5 Å distance obtained

Table 1. DFT Calculated and Experimental e^2qQ Values for ^{43}Ca and ^{87}Sr Ions in Various Protein Sites

| | <i>a</i> | <i>b</i> | <i>c</i> | reference |
|--------------------------------|--------------------------------------|------------------|------------------|------------|
| | DFT Calculated Values e^2qQ in MHz | | | |
| metal ion | ^{43}Ca | ^{87}Sr | ^{87}Sr | |
| site 1 | 0.53 | 14.5 | 31.4 | |
| site 2 | 1.54 | 26.0 | 37.6 | |
| site 3 | 1.48 | 25.1 | 39.2 | |
| site 4 | 2.80 | 18.7 | | |
| | Available Literature Data | | | |
| PPLA2 | 0.76–0.78, (0.79) ^d | | | 54, 55, 56 |
| PLA2 | 0.84–1.79 (1.61–2.33) ^d | | | 54, 55, 56 |
| parvalbumin | 1.3 | | | 57 |
| calmodulin | 1.15 | | | 57 |
| calmodulin | 1.22 | | | 58 |
| troponin C | 1.05 | | | 57 |
| α -lactalbumin (bovine) | 0.70 | | | 59 |
| α -lactalbumin (human) | 0.81 | | | 58 |
| lysozyme (equine) | 0.75 | | | 58 |
| lysozyme (pigeon) | 0.69 | | | 58 |

^a Coordinates from the crystal structures. ^b Ca/Sr substituted in the coordinates from the crystal structures. ^c Fully optimized model sites. ^d The e^2qQ value in parentheses is reported for a “weak” binding site.

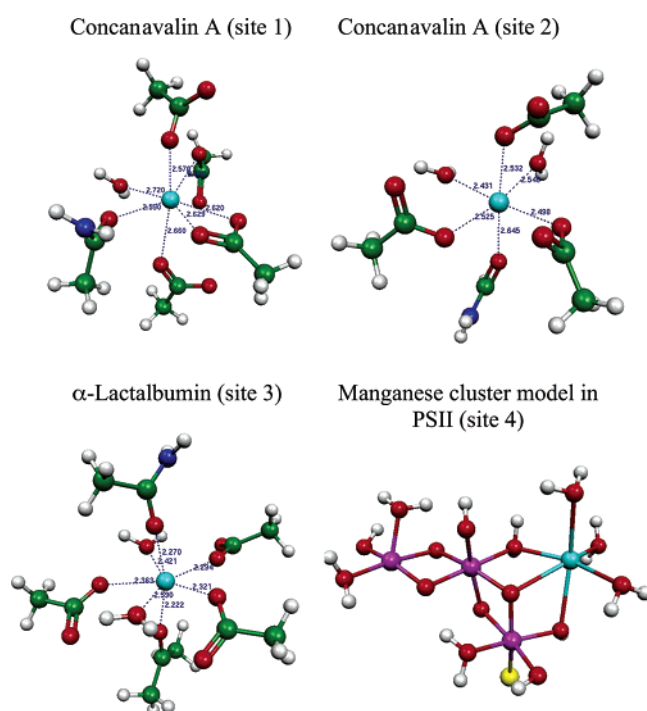


Figure 5. Schematic representation of the Ca binding sites used for the calculations of the Sr and Ca quadrupolar couplings. Coordinates of sites 1–3 were extracted from crystal structures of concanavalin A and α -lactalbumin. The trinuclear Mn plus Ca core of site 4 was constructed and partially optimized according to ref 53. Colors used for different atoms: hydrogen - white, oxygen - red, carbon - green, nitrogen - dark blue, calcium - light blue, manganese - violet, chlorine - yellow.

in the low quadrupolar coupling limit simulation is calculated using a single-point dipole approximation. This Mn– ^{87}Sr point dipolar distance is thus only a rough estimation, and the actual link between the dipolar and distances will depend on the orientation of the various Mn-nucleus vectors with respect to the cluster and its distributed spin density. To better interpret the distance between the calcium/strontium binding site and the Mn cluster, we employed a multiple-point dipole methodology as in previous papers.^{32–33,60} For a multinuclear metal cluster,

it is important to consider the effects of electron spin distributed among the metal ions. Therefore, each manganese contributes additively to the total dipolar coupling tensor:

$$A_{\text{dip}}^{\text{total}} = \sum_i \rho_i (A_{\text{dip}})_i \quad (9)$$

where ρ is the spin projection factor that converts each ion (i) from an uncoupled basis set to a coupled basis set. Consequently, the projection factors depend on the oxidation state of each manganese ion and the exchange coupling scheme used to model the manganese ion spin states. A_{dip} is calculated over the three-dimensional space about a given structural and magnetic model of the Mn cluster. This procedure can generate the contour surfaces of constant dipolar coupling.

Figure 6 shows planar slices through the contours of constant dipolar hyperfine coupling $A_{\text{dip}} = 0.038$ MHz, the value used in our simulations of Figure 3, based on our “dangler” 3 + 1 structural model (*vide supra*). Utilizing the contour map, we can estimate a range of possible distances from the calcium/strontium binding site to the nearest Mn ion to the cluster. We find a range of 3.8–5.0 Å corresponding to the dipolar hyperfine coupling $A_{\text{dip}} = 0.038$ MHz we used in the simulation.

The distance between the Mn cluster and the Sr^{2+} (Ca^{2+}) binding site calculated here is somewhat larger than the previous EXAFS results, but this should be considered an upper limit range based on our previous discussion of quadrupolar effects. However we note that the distances estimated here are quite similar to the metal–metal distances seen in the calcium-containing metalloenzymes. The manganese–calcium binding site of concanavalin A has a metal–metal distance of 4.2 Å,⁶¹ and two calcium ions in thermolysin are found with the distance of 3.8 Å.⁶²

(54) Drakenberg, T.; Andersson, A.; Forsén, S.; Wieloch, T. *Biochemistry*, **1984**, *23*, 2387–2392.

(55) Andersson, A.; Drakenberg, T.; Forsén, S.; Wieloch, T.; Lindstrom, M. *FEBS Lett.* **1981**, *123*, 115–117.
 (56) Forsén, S.; Andersson, A.; Drakenberg, T.; Thulin, E.; Sword, M. *Fed. Proc.* **1982**, *41*, 2981–2986.
 (57) Andersson, A.; Drakenberg, T.; Forsén, S.; Thulin, E.; Sword, M. *J. Am. Chem. Soc.* **1982**, *104*, 576–580.
 (58) Malmendal, A.; Linse, S.; Evenes, J.; Forsén, S.; Drakenberg, T. *Biochemistry* **1999**, *38*, 11844–11850.
 (59) Aramini, J. M.; Drakenberg, T.; Hiraoki, T.; Ke, Y.; Nitta, K.; Vogel, H. *J. Biochemistry* **1992**, *31*, 6761–6768.
 (60) Randall, D. W.; Gelasco, A.; Caudle, M. T.; Pecoraro, V. L.; Britt, R. D. *J. Am. Chem. Soc.* **1997**, *119*, 4481–4491.

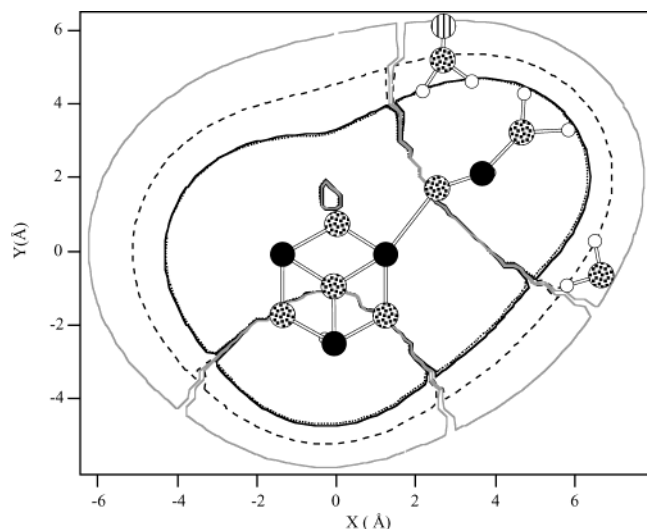


Figure 6. Molecular model of the calcium/strontium binding site of the manganese cluster, superimposed on the constant hyperfine slice through $A_{\text{dip}} = 0.038$ MHz (solid line) ^{87}Sr hyperfine isosurfaces using the “Dangler model”. The projection factors for the manganese atoms from left to right are 1.22, -0.95 , 1.62, and -0.90 .^{9,33} For a possible nucleophile model of the calcium/strontium, ^2H values are included with the isosurfaces of $A_{\text{dip}} = 0.64$ MHz (dotted black line), $A_{\text{dip}} = 0.61$ MHz (solid black line), and $A_{\text{dip}} = 0.30$ MHz (broken black line). The positions of the protons or water molecules were determined from the simultaneous analysis of the ENDOR and ESEEM (two- and three-pulse) data.⁶³ See more details in the text. Atom key: Mn (black solid), O (dotted), H (white circle) and Sr (striped).

In addition, the calcium/strontium binding site can be well incorporated with the positions of the protons or water molecules determined from the simultaneous analysis of the ENDOR and ESEEM⁶³ as shown in Figure 6. This interpretation of the distance of the calcium/strontium binding site to the Mn cluster estimated here is consistent with the calcium-nucleophile model in which one substrate water binds to the calcium cofactor (see Figure 6). Pecoraro and co-workers⁶⁴ and Brudvig and co-workers⁶⁵ proposed models in which the Mn bound species is highly electrophilic, for example, a Mn(V)=O , that is subject to nucleophilic attack by the calcium bound substrate. However, we certainly cannot rule out other possible roles for a proximal Ca/Sr ion.

In conclusion, the ^{87}Sr three-pulse ESEEM results clearly reveal that the calcium binding site in the OEC is close to the

Mn cluster. The data and conclusions from this ^{87}Sr magnetic resonance experiment are arrived at fully independently from previous X-ray spectroscopic and X-ray diffraction approaches. The complementary results here confirm the presence of a Ca/Sr binding site in close proximity to the Mn cluster, as has been argued on the basis of a number of EXAFS experiments.

Conclusions

We exploited ^{87}Sr three-pulse ESEEM to examine whether the Ca^{2+} binding site of PSII is close to the Mn cluster in the OEC. In addition to obtaining the modified multiline of strontium-reconstituted PSII membranes, three-pulse ESEEM experiments on enriched ^{87}Sr -reconstituted samples clearly showed modulation arising from strontium in the time domain as well as a peak at 0.64 MHz, corresponding to the ^{87}Sr Larmor frequency in the frequency domain of three-pulse ESEEM. Analysis of the ^{87}Sr three-pulse ESEEM experiments yields a distance between the Mn cluster and the Ca^{2+} (Sr^{2+}) binding site in the OEC of ca. 4.5 Å using the analytical expression of three-pulse ESEEM with the absence of quadrupolar effect. The simulation of three-pulse ESEEM using matrix diagonalization showed a good agreement with the analytical expression result and suggested a relatively small quadrupolar coupling for ^{87}Sr in this site. These results together with DFT calculations of ^{43}Ca and ^{87}Sr quadrupolar interactions on Ca (and Sr substituted) binding sites suggest a highly symmetrical ligand environment for the Sr^{2+} -substituted Ca site. In addition, utilizing multiple-point dipole methodology we estimated a maximum distance range of 3.8–5.0 Å from the calcium/strontium binding site to the nearest Mn ion to the tetra-Mn cluster.

This work provides direct evidence that the calcium binding site is close to the Mn cluster in the OEC.

Note in Revision. We note that a new *Thermosynechococcus elongatus* PSII structure with slightly improved resolution (3.5 Å) has recently appeared in online form.⁶⁶ The structural refinement shows a 3Mn + 1Mn structure similar to the “dangler” structure employed in this paper. What is new on the calcium forefront is the assignment of electron density to Ca within the core, forming a 3Mn–Ca cluster. This is certainly consistent with the <4.5 Å distance to calcium proposed by this work. We are working on spectral and DFT simulations based on this latest proposed structure.

Acknowledgment. This work was supported by NIH Grant GM48242. We would like to thank Dr. Keri Clemens for helpful discussions about the sample preparation and Dr. Constantino Aznar for providing the contour plot. We also gratefully appreciate Professor Kurt Warncke for providing the ESEEM code. The work of M. Brynda was supported by Swiss National Science Foundation Grant 8220-067593.

JA030614E

- (61) (a) Edelman, G. M.; Cunningham, B. A.; Reeke, G. N.; Becker, J. W.; Waxdal, M. J.; Wang, J. L. *Proc. Natl. Acad. Sci. U.S.A.* **1972**, *69*, 2580–2584. (b) Hardman, K. D.; Ainsworth, C. F. *Biochemistry* **1972**, *11*, 4910–4919.
- (62) Matthews, B. W.; Weaver, L. H.; Kester, W. R. *J. Biol. Chem.* **1974**, *249*, 8030–8044.
- (63) (a) Aznar, C. P.; Britt, R. D. *Philos. Trans. R. Soc. London, Ser. B* **2002**, *357*, 1359–1366. (b) Britt, R. D.; Campbell, K. A.; Peloquin, J. M.; Gilchrist, M. L.; Aznar, C. P.; Dicus, M. M.; Robblee, J.; Messinger, J. *Biochim. Biophys. Acta*, submitted.
- (64) Pecoraro, V. L.; Baldwin, M. J.; Caudle, M. T.; Hsieh, W.; Law, N. A. *Pure Appl. Chem.* **1998**, *70*, 925–929.
- (65) Limberg, J.; Szalai, V. A.; Brudvig, G. W. *J. Chem. Soc., Dalton Trans.* **1999**, 1353–1361.

- (66) Ferreira, K. N.; Iverson, T. M.; Maghlaoui, K.; Barber, J.; Iwata, S. *Science*, in press.